RAA 2014 Vol. **14** No. **1**, 66–76 doi: 10.1088/1674–4527/14/1/005
http://www.raa-journal.org *http://www.iop.org/journals/raa*

***R**esearch in*
***A**stronomy and*
***A**strophysics*

Evolution of filamentary molecular clouds in the presence of magnetic fields

Alireza Khesali[1], Khodadad Kokabi[1], Kazem Faghei[2] and Mohsen Nejad-Asghar[1]

[1] Department of Physics, University of Mazandaran, Babolsar 47416-95447, Iran; *kh.kokabi@umz.ac.ir*
[2] School of Physics, Damghan University, Damghan 36716-41167, Iran

Received 2013 February 24; accepted 2013 September 5

Abstract The purpose of this paper is to explore the effect of magnetic fields on the dynamics of magnetized filamentary molecular clouds. We suppose there is a filament with cylindrical symmetry and two components of axial and toroidal magnetic fields. In comparison to previous works, the novelty in the present work involves a similarity solution that does not define a function of the magnetic fields or density. We consider the effect of the magnetic field on the collapse of the filament in both axial and toroidal directions and show that the magnetic field has a braking effect, which means that the increasing intensity of the magnetic field reduces the velocity of collapse. This is consistent with other studies. We find that the magnetic field in the central region tends to be aligned with the filament axis. Also, the magnitude and the direction of the magnetic field depend on the magnitude and direction of the initial magnetic field in the outer region. Moreover, we show that more energy dissipation from the filament causes a rise in the infall velocity.

Key words: ISM: clouds — ISM: magnetic fields

1 INTRODUCTION

Giant Molecular Clouds (GMCs) are one of the most important sites of star formation. There are filamentary structures in most molecular clouds. If we suppose that filamentary structures have been formed from GMCs, then their interactions would be a useful way to investigate star formation. Since filamentary structures have been observed with cores and clumps, it seems that formation and fragmentation of filaments are the most important steps in the process of star formation.

Chandrasekhar & Fermi (1953) studied the stability of a non-condensed self-gravitating filament which is in equilibrium, according to the cylindrical symmetry of the fluid. Also, Stodólkiewicz (1963) and Nagasawa (1987) considered the stability of isothermal, magnetized filaments. They assumed the same density distribution, $\rho_0 = \rho_c(1 + \frac{r^2}{H^2})^{-2}$, though the expression for H (scale height) is different. Nakajima & Hanawa (1996) assumed the density distribution is expressed as $\rho = \rho_0 \sec h^2(\frac{y}{H})$. Miyama et al. (1987) discovered that the infall velocity is proportional to the distance from the axis for an unmagnetized isothermal cylinder and its density profile is similar to that of the Stodólkiewicz case in which the scale radius decreased and central density increased with time.

Various physical processes such as self-gravity, thermal processes and magnetic fields play the main roles in star formation (Larson 1985; Nakamura et al. 1995; Nakajima & Hanawa 1996; Tilley & Pudritz 2003; Shadmehri 2005; Schneider et al. 2010).

The observed magnetic fields show various configurations with respect to the filament axes (Poidevin et al. 2011). In some clouds, like Taurus (Moneti et al. 1984) and Lupus 1 (Strom et al. 1988), the magnetic field is roughly perpendicular to the filament axes. In other clouds, like Ophiuchus (Vrba et al. 1976) and the R CrA cloud (Vrba et al. 1981), the magnetic field is roughly parallel to the filament axes. Bally (1989) and Uchida (1989) suggested that the L1641 region of the Orion molecular cloud is penetrated by a helical magnetic field winding around the filament in a right-handed helix (as seen from the direction of Ori KL) (Uchida et al. 1991).

Magnetic fields have been shown to be energetically comparable to gravity and kinetic motions within molecular clouds (Myers & Goodman 1988a,b; Crutcher et al. 1999), and are theorized to provide vital support to clouds in preventing global collapse. Hennebelle (2003) explored a self-similar solution for a rotating, magnetized filament that collapses in the direction of the axis. Tilley & Pudritz (2003) presented an isothermal self-similar solution for the magnetic filament. Due to the constant toroidal flux to mass ratio, they found that a weak magnetic field resulted in a profile of the density described as $\rho \propto r^{-4}$ and $\rho \propto r^{-2}$ (behavior of the strong field) for large radius. Shadmehri (2005) considered the gravitational collapse of a polytropic magnetized filamentary cloud and he studied the effect of the toroidal component of the magnetic field in the collapse of the filament. He showed that the radial velocity does not play such a simple role.

According to the different magnetic fields that have been observed in molecular clouds, our goal is to extend the calculations describing self-similar collapse of a magnetized, filamentary molecular cloud. Some researchers (Nagasawa 1987; Miyama et al. 1987; Nakamura et al. 1999; Tilley & Pudritz 2003) have introduced a function for the cloud density and some of them introduced a function for the magnetic field to simplify the equations in which some of them have used it in the z-direction and others in the $z - \varphi$ direction. In this work, according to observations in the outer region of the filamentary cloud, we want to calculate the strength of the magnetic field components in the other regions of the cloud by selecting a magnetic field in the z and φ directions. Moreover we consider the effect of this magnetic field on the other parameters of the filament such as density, pressure, etc. We want to use the energy equation for studying the effects of the magnetic field in the collapse of the magnetized filamentary molecular cloud by using the self-similar solution. In addition, we investigate the effects of variations in the cooling function on the filamentary molecular clouds.

We present the general formulation in Section 2. The self-similar solution of the model is shown in Section 3. The magnetosonic singularity is considered in Section 4 and we describe the initial and boundary conditions and numerical procedures in Section 5. We obtain the asymptotic solutions in Section 6. In Section 7 we summarize our results.

2 GENERAL FORMULATION

In this section, considering the symmetry of the problem, we regard the cloud to be a long cylinder in which its axis is the z-axis; also, the magnetic field is defined as $\boldsymbol{B} = B_\varphi \boldsymbol{\varphi} + B_z \boldsymbol{k}$ so that B_z and B_φ depend on the radial distance (r) and time.

A molecular cloud exchanges energy with its environment. Processes such as cosmic ray interaction, a diffuse radiation field, dust irradiation, photoelectric ejection and carbon ionization cause an increase in the heat of the cloud. Moreover, stellar X-rays are another factor heating the cloud with ionizing hydrogen. Mechanisms like the inelastic interactions between hydrogen or helium and atoms, molecules or dust decrease the energy by emission of photons. The interstellar dust is also one of the most important agents in the cooling mechanism with emission of IR photons. In this paper, these factors are expressed as a net cooling function in the energy equation.

According to the ideal gas and energy equations, the basic equations are as follows:

$$\frac{\partial \rho}{\partial t} + \frac{1}{r}\frac{\partial}{\partial r}(r\rho v) = 0, \tag{1}$$

$$\rho\left(\frac{\partial v}{\partial t} + v\frac{\partial v}{\partial r}\right) = -\frac{\partial p}{\partial r} - \rho\frac{\partial \psi}{\partial r} - \frac{1}{4\pi}\left[B_z\frac{\partial B_z}{\partial r} + \frac{1}{r}B_\varphi\frac{\partial}{\partial r}(rB_\varphi)\right], \tag{2}$$

$$\frac{1}{r}\frac{\partial}{\partial r}\left(r\frac{\partial \psi}{\partial r}\right) = 4\pi G\rho\,, \tag{3}$$

$$\frac{\partial \boldsymbol{B}}{\partial t} = \boldsymbol{\nabla}\times(\boldsymbol{v}\times\boldsymbol{B})\,, \tag{4}$$

$$\frac{1}{\gamma-1}\left[\frac{\partial p}{\partial t} + v\frac{\partial p}{\partial r}\right] + \frac{\gamma}{\gamma-1}\frac{p}{r}\frac{\partial}{\partial r}(rv) + A_\nu\rho^2T^\nu = 0, \tag{5}$$

$$p = \frac{R}{M}\rho T, \tag{6}$$

where ρ, v, p, ψ, B and T denote the gas density, radial velocity, pressure, gravitational potential, magnetic field and temperature, respectively. Also υ and A_υ are constants that depend on the selected intervals of temperature (Spitzer 1978). All of the variations depend on r, the distance from the cylindrical axis, and time.

To simplify the problem, we introduce the dimensionless variables according to

$$\begin{aligned} &\rho \longrightarrow \hat{\rho}\rho, \quad t \longrightarrow \hat{t}t, \quad v \longrightarrow \hat{v}v, \quad r \longrightarrow \hat{r}r, \\ &p \longrightarrow \hat{p}p, \quad \psi \longrightarrow \hat{\psi}\psi, \quad B \longrightarrow \hat{B}B, \quad T \longrightarrow \hat{T}T, \end{aligned} \tag{7}$$

where

$$\begin{aligned} \hat{\rho} &= \rho_0, \quad \hat{p} = p_0, \quad \hat{\psi} = \frac{\hat{p}}{\hat{\rho}}, \quad \hat{r} = \left(\frac{\hat{p}}{4\pi G\hat{\rho}}\right)^{\frac{1}{2}}, \\ \hat{t} &= \frac{\hat{p}}{A_\nu\hat{\rho}^2\hat{T}^\nu}, \quad \hat{v} = \frac{\hat{r}}{\hat{t}}, \quad \hat{B} = (4\pi\hat{p})^{\frac{1}{2}}. \end{aligned} \tag{8}$$

We measure the length and time in units of 1 pc and 10^6 yr, respectively, so that the velocity unit is 1 km s^{-1}. The unit of mass is defined to be 1 $M_\odot$, thus the gravitational constant is $G = 4.48 \times 10^{-3}$. In this manner, the units of temperature and density are 130 K and 6.67×10^{-23} gr cm^{-3}, respectively. Finally, the unit of magnetic field is chosen to be equal to 2.85 μG.

As mentioned above, the goal of this research is to explore how the behavior of the physical quantities evolves with time and local variations. Although an exact illustrative solution is impossible, a numerical method can describe the overall behavior.

In this work we use the self-similar method that will be described in the following sections.

3 SELF-SIMILAR SOLUTION

By transforming Equation (7), we can make the following substitutions to change our dimensionless variables from functions of (r,t) to separable functions of (η,t), for the self-similar variable $\eta = r/t^n$. We also use the following forms for the physical variables:

$$\rho(r,t) = R(\eta)t^{\epsilon_1}\,, \tag{9}$$

$$v(r,t) = V(\eta)t^{\epsilon_2}\,, \tag{10}$$

$$\psi(r,t) = \phi(\eta)t^{\epsilon_3}\,, \tag{11}$$

$$B_z(r,t) = b_z(\eta)t^{\epsilon_4}\,, \tag{12}$$
$$B_\varphi(r,t) = b_\varphi(\eta)t^{\epsilon_5}\,, \tag{13}$$
$$p(r,t) = P(\eta)t^{\epsilon_6}\,. \tag{14}$$

By equilibrating the time powers, local equations will be defined as follows:

$$\epsilon_1 R - n\eta\frac{\partial R}{\partial \eta} + \frac{1}{\eta}\frac{\partial}{\partial \eta}(\eta R V) = 0, \tag{15}$$

$$\epsilon_2 V - n\eta\frac{\partial V}{\partial \eta} + V\frac{\partial V}{\partial \eta} = -\frac{1}{R}\frac{\partial P}{\partial \eta} - \frac{\partial \phi}{\partial \eta} - \frac{b_z}{R}\frac{\partial b_z}{\partial \eta} - \frac{b_\varphi}{R\eta}\frac{\partial}{\partial \eta}(\eta b_\varphi), \tag{16}$$

$$\frac{1}{\eta}\frac{\partial}{\partial \eta}\left(\eta\frac{\partial \phi}{\partial \eta}\right) = R, \tag{17}$$

$$\epsilon_5 b_\varphi - n\eta\frac{\partial b_\varphi}{\partial \eta} + \frac{\partial}{\partial \eta}(V b_\varphi) = 0, \tag{18}$$

$$\epsilon_4 b_z - n\eta\frac{\partial b_z}{\partial \eta} + \frac{1}{\eta}\frac{\partial}{\partial \eta}(\eta V b_z) = 0, \tag{19}$$

$$\frac{1}{\gamma - 1}\left(\epsilon_6 P - n\eta\frac{\partial P}{\partial \eta} + V\frac{\partial P}{\partial \eta}\right) + \frac{\gamma}{\gamma - 1}\frac{P}{\eta}\frac{\partial}{\partial \eta}(\eta V) + R^{2-\nu}P^\nu = 0, \tag{20}$$

where ϵ_1-ϵ_6 and n are obtained as follows:

$$\epsilon_1 = -2\,, \tag{21}$$
$$\epsilon_3 = 2\epsilon_2 = \frac{1}{\nu - 1}\,, \tag{22}$$
$$\epsilon_6 = 2\epsilon_4 = 2\epsilon_5 = -\frac{2\nu - 3}{2\nu - 2}\,, \tag{23}$$
$$n = \frac{2\nu - 1}{2\nu - 2}. \tag{24}$$

Now Equations (15)–(20) can be solved by using the fourth-order Runge-Kutta method which is explored in the next sections.

4 MAGNETOSONIC SINGULARITY

Combining all reduced Equations (15)–(20), we readily derive six coupled non-linear ordinary differential equations (ODEs) for V, R, P, b_z, b_φ and ϕ as

$$\frac{dR}{d\eta} = \frac{\epsilon_1 R\eta + RV}{\eta(n\eta - V)} - \frac{RA_1}{\eta(V - n\eta)A_2}\,, \tag{25}$$
$$\frac{dV}{d\eta} = \frac{A_1}{\eta A_2}\,, \tag{26}$$
$$\frac{d\phi'}{d\eta} = -\frac{\phi' - R\eta}{\eta}\,, \tag{27}$$

$$\frac{db_z}{d\eta} = \frac{\epsilon_4\eta b_z + Vb_z}{\eta(n\eta - V)} - \frac{b_z A_1}{\eta(V - n\eta)A_2}\,, \tag{28}$$

$$\frac{db_\varphi}{d\eta} = \frac{\epsilon_5 b_\varphi}{n\eta - V} - \frac{b_\varphi A_1}{\eta(V - n\eta)A_2}\,, \tag{29}$$

$$\frac{dP}{d\eta} = \frac{\left(\left(b_\varphi^2 - R(V - n\eta)^2\right) + b_z^2\right) A_1}{\eta(V - n\eta)A_2} + \frac{\left(\left(\epsilon_5 b_\varphi^2 - (V - n\eta)\left(\epsilon_2 RV + \frac{b_\varphi^2}{\eta} + R\phi'\right)\right) + b_z\left(\epsilon_4 b_z + \frac{Vb_z}{\eta}\right)\right)}{V - n\eta}\,, \tag{30}$$

where

$$A_1 = R^{-\nu}(\epsilon_2 nV\eta^2 R^{\nu+1} - \epsilon_2 V^2\eta R^{\nu+1} + \epsilon_4\eta b_z^2 R^\nu + \epsilon_5\eta b_\varphi^2 R^\nu + \epsilon_6 P\eta R^\nu + n\phi'\eta^2 R^{\nu+1} + n\eta b_\varphi^2 R^\nu + \gamma R^2\eta P^\nu - R^2\eta P^\nu + \gamma PVR^\nu - \phi' V\eta R^{\nu+1} - Vb_\varphi^2 R^\nu + Vb_z^2 R^\nu)\,, \tag{31}$$

$$A_2 = R(V - n\eta)^2 - b_\varphi^2 + b_z^2 + \gamma P. \tag{32}$$

For smooth, regular solutions crossing the magnetosonic line (Lou & Shen 2004), the critical conditions are

$$V - n\eta = 0, \tag{33}$$

$$(V - n\eta)^2 - \frac{b_\varphi^2 + b_z^2 + \gamma P}{R} = 0. \tag{34}$$

Since the radial velocity in the present model is negative and $n\eta > 0$, $V - n\eta \neq 0$. Equation (34) is equivalent to the magnetosonic condition (Yu & Lou 2005). When the magnetosonic condition is satisfied, a singularity arises. For $\eta > 0.1$, the density of the filament becomes smaller than the density of the interstellar medium. Therefore, Equation (34) does not satisfy the condition $(V - n\eta)^2 - \frac{b_\varphi^2 + b_z^2 + \gamma P}{R} \neq 0$ from the center to cloud radius ($0 < \eta \leq 0.1$). Thus we do not have any singularity in this region. According to Figures 4, 7 and 8, the curved magnetosonic critical lines and the curved lines that describe infall velocity do not intersect, i.e. no singularity arises.

5 INITIAL AND BOUNDARY CONDITIONS AND NUMERICAL PROCEDURES

In this section, by using observed boundary conditions, we integrate Equations (15)–(20) from the outer to the inner regions and survey the corresponding change in quantities.

Some authors have suggested that filamentary structures occur as a result of the fragmentation of the parent molecular clouds through turbulent motions (Nakamura et al. 1995; Nakajima & Hanawa 1996; Klessen & Burkert 2000; Ostriker et al. 2001). To be consistent with observations of filamentary molecular clouds, the density in the central region should be higher than that in the outer region. The filamentary molecular cloud density is low in the outer region, and has the same density as the interstellar medium. For this reason we select the typical number density $n = 10\,\mathrm{m_{H_2}}\ \mathrm{cm}^{-3}$. Nakajima & Hanawa (1996) used the density in the central region of $n = 10^4\ \mathrm{m_{H_2}}\ \mathrm{cm}^{-3}$ for a typical filament which according to observations (Li & Goldsmith 2012; Henshaw et al. 2013) should be about $10^3 - 10^4\ \mathrm{m_{H_2}}\ \mathrm{cm}^{-3}$.

By using the boundary conditions and free parameter ν that is selected from the cooling function, we can solve the set of ODEs. We can assume an initial value of $\nu = 2.4$ for a typical cloud and determine the other parameters corresponding to that amount (Goldsmith 2001).

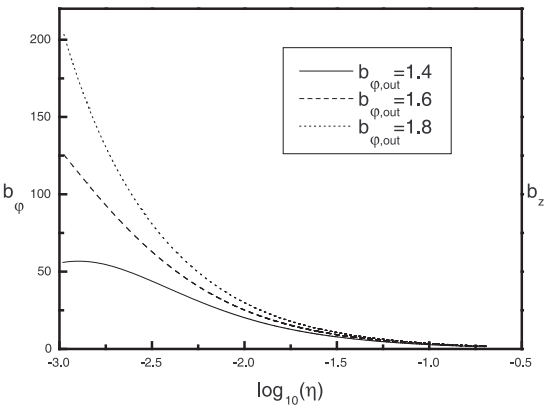

Fig. 1 Profile of the toroidal component of the magnetic field corresponding to $\gamma = 1.66$, $b_{z,\mathrm{out}} = 0.1$ and a different initial value for the toroidal component of magnetic field.

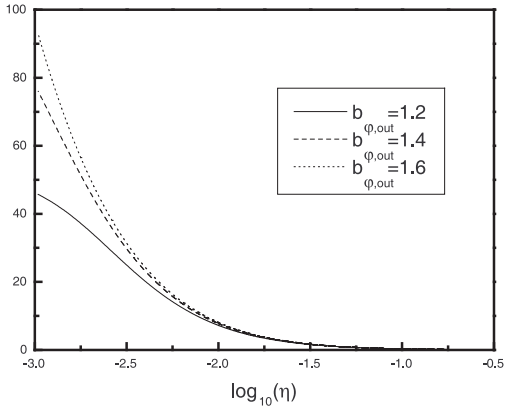

Fig. 2 Same as Fig. 1, but for the axial component of the magnetic field.

As deduced from observations, the magnetic field can assume different shapes in filamentary molecular clouds that make a different angle with the axis in the outer region of the filament. Fiege & Pudritz (2000) showed that the toroidal component of the magnetic field in the outer region of the filament dominates the other components when the models consist of poloidal and toroidal magnetic fields. To achieve a good approximation, Tilley & Pudritz (2003) assumed that the magnetic field in the outer region of the filament is purely toroidal. Shadmehri (2005) assumed that the toroidal component of the magnetic field is dominant. Because the toroidal magnetic field in the outer region is dominant, we assume that the initial axial component of the magnetic field is smaller than the toroidal component for the outer region. Also, the strength of the magnetic field in the magnetized filament is on the order of micro Gauss. For example, the local interstellar medium has a magnetic field strength of 4 μG (Opher et al. 2009). The Radio Arc filaments have been estimated to have a magnetic field strength of 10 μG (Ferrière 2009; Chapman et al. 2011).

The typical value of temperature in the outer region of a cloud is approximately 10 K. Thus, using this value of temperature, the dimensionless form of sound speed in this region becomes 1. The infall velocity in the outer region is less than 3 km s^{-1} (Nakamura et al. 1995), so we select the typical dimensionless infall velocity in the outer region to be $V = -0.5$.

We can calculate variations in the magnetic field using typical values for components of the magnetic field. Firstly, we consider the effect of the initial condition of the magnetic field's toroidal component, b_φ, on variations in the field. Therefore, the increases of the magnetic field in the central region of the filament are consistent with the latest works (Fiege & Pudritz 2000; Tilley & Pudritz 2003; Shadmehri 2005). Also, if the magnetic field's toroidal component in the outer region is greater, components of the magnetic field increase in the center of the filament (Figs. 1 and 2).

According to the latest works and observations (Tilley & Pudritz 2003; Shadmehri 2005; Poidevin et al. 2011) the magnetic field in the outer region is toroidal. By approaching the central region, we observed that the $\alpha = b_\varphi / b_z$ ratio in Figure 3 decreases, i.e. the magnetic field tends to be directed along the filament axis, which is consistent with Nakajima & Hanawa (1996).

Tilley & Pudritz (2003) showed that in the isothermal case the radial velocity is proportional to the radial distance, which means in the central region V is very low. Shadmehri (2005) showed that there is no relationship between V and r in the polytropic case, but the infall velocity near the axis is very small and it increases toward the outer region. We have incorperated these variations into the infall velocity.

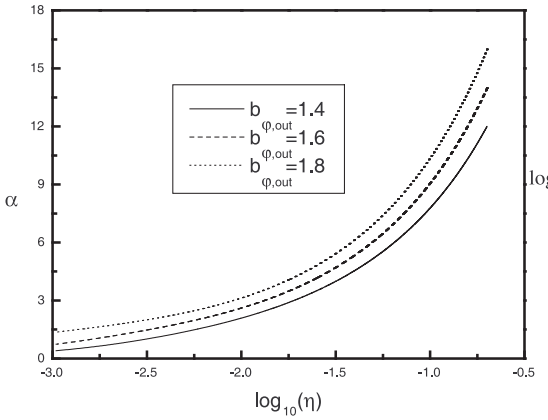

Fig. 3 Ratio of toroidal component of the magnetic field to the axial component corresponding to $\gamma = 1.66$ and $b_{z,\mathrm{out}} = 0.1$.

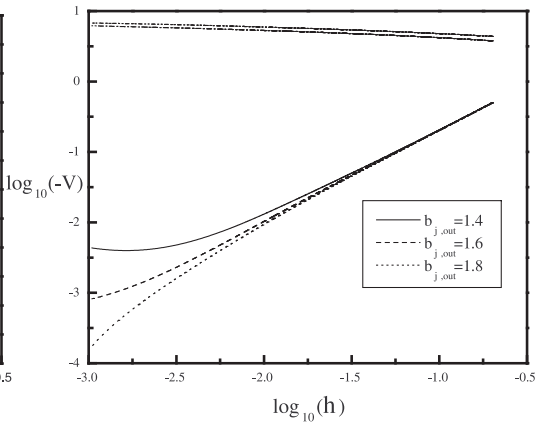

Fig. 4 Velocity distribution in the similarity solution for $\gamma = 1.66$. It shows the magnetic field is having a braking effect. The above two lines are the curved magnetosonic critical lines.

To consider the effect of the magnetic field on the variation of velocity, we studied the toroidal component in which we expect that increasing the magnetic field strength leads to decreasing the infall velocity; with increasing distance from the axis the infall velocity increases, which is shown in Figure 4, assuming $\gamma = 1.66$ and we change the initial value of the toroidal component of the magnetic field. Also, its negative sign shows the direction of velocity with respect to the axis, i.e. the molecular cloud is collapsing, which is consistent with other works (Larson 1985; Shadmehri 2005).

Therefore, increasing the B reduces the infall velocity, which shows that the magnetic field helps the pressure gradient against gravity and it has a magnetic braking effect that is consistent with Nakajima & Hanawa (1996) and Shadmehri (2005).

Figure 4 also confirms these results. Nagasawa (1987), Tilley & Pudritz (2003) assumed the density distribution is a function of radius in which increasing the radius decreases the density. Shadmehri (2005) considered the self-similar solution for magnetized filamentary clouds by the toroidal component and showed that the toroidal component of the magnetic field helps to confine the gas by hoop stress. We include the density profile and the effect of the magnetic fields in the variation of the density.

Figure 5 shows the value of the density which increases from the outer region to the central region that is consistent with observations and the latest works. With the magnitude of the toroidal magnetic field component increasing, the density increases, which is consistent with Shadmehri (2005). So, we show that increasing the magnetic field increases the density (Chapman et al. 2011).

Regarding Figure 6, it can be observed that even though we proceed from the outer region of the filament to the center, the temperature stays stable, which is consistent with observations (Li & Goldsmith 2003; Miettinen & Harju 2010). Also, according to the constraint that the pressure in the filament should be equal to the total thermal and magnetic pressure, with the growth of magnetic pressure, thermal pressure will grow less and because the temperature is proportional to the thermal pressure with the expansion of the magnetic field in the outer region of the filament, it is obvious that with a smaller filament radius, the temperature grows less.

We expect that, in the process of filament collapse when more energy is released from the filament, the infall velocity is increased. Because we introduced the net cooling as a function, increasing ν increases the infall velocity (Fig. 7).

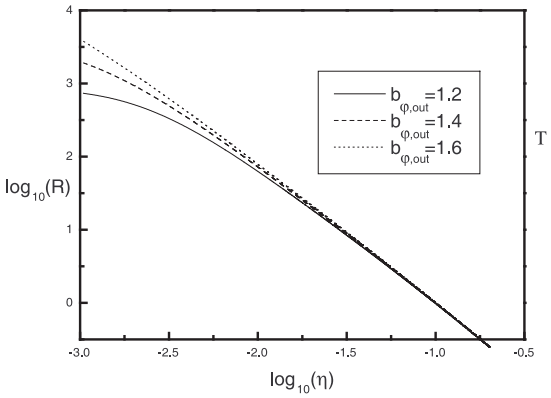

Fig. 5 Density profile corresponding to $\gamma = 1.66$, $b_{z,\mathrm{out}} = 0.1$ and different initial values for the toroidal component of the magnetic field.

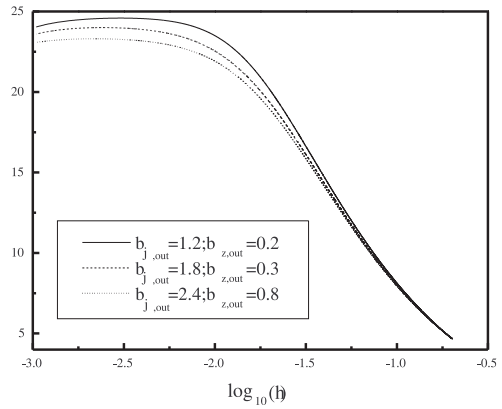

Fig. 6 Temperature profile corresponding to $\gamma = 1.66$ and a different initial value for the magnetic field.

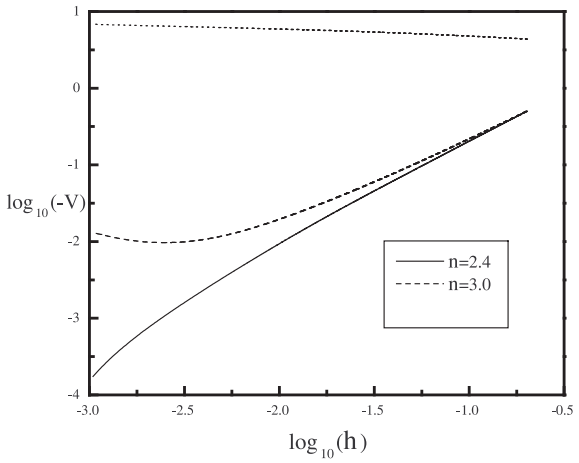

Fig. 7 Velocity distribution in the similarity solution for $b_{\varphi,\mathrm{out}} = 1.8$, $b_{z,\mathrm{out}} = 0.1$, $\nu = 2.4$ and $\nu = 3.0$ that shows the effect of the cooling function. The above line is the curved magnetosonic critical line.

6 ASYMPTOTIC SOLUTIONS

In the previous section, we used the observational data to set the initial conditions for equations describing the system and integrate them from the outer to the inner regions. To test the accuracy of these results, the asymptotic behavior of Equations (15)–(20) as $\eta \longrightarrow 0$ is investigated. We apply the asymptotic result as the inner boundary conditions to integrate from the inner to the outer regions. In order to obtain asymptotic behavior, we can substitute the series below in Equations (15)–(20)

$$R(\eta) \sim (R_0 + R_1\eta)\eta^{\alpha_1}\,, \tag{35}$$
$$V(\eta) \sim V_1\eta^{\alpha_2+1}\,, \tag{36}$$
$$b_z(\eta) \sim \lambda(b_{z0} + b_{z1}\eta)\eta^{\alpha_3}\,, \tag{37}$$
$$b_\varphi(\eta) \sim \lambda(b_{\varphi 0} + b_{\varphi 1}\eta)\eta^{\alpha_4}\,, \tag{38}$$

$$\phi(\eta) \sim (\phi_0 + \phi_1\eta)\eta^{\alpha_5}\,, \tag{39}$$
$$P(\eta) \sim (P_0 + P_1\eta)\eta^{\alpha_6}\,, \tag{40}$$

where V_1, R_0 and λ are three constant parameters referred to as the velocity, density and magnetic field strength, respectively. The rest of the parameters are obtained as:

$$\alpha_1 = \frac{\epsilon_1}{n}, \qquad \alpha_2 = 1, \qquad \alpha_3 = \alpha_4 = \frac{\epsilon_4}{n}\,, \tag{41}$$
$$\alpha_5 = \alpha_1 + 2, \qquad \alpha_6 = 2\alpha_1 + 2\,, \tag{42}$$

$$R_1 = \frac{(3+\alpha_1)R_0V_1}{n}, \tag{43}$$

$$\phi_0 = \frac{R_0}{\alpha_5^2}, \qquad \phi_1 = \frac{R_1}{(\alpha_5+1)^2}, \tag{44}$$
$$P_0 = -\frac{R_0^2}{\alpha_5\alpha_6}, \qquad P_1 = -\frac{R_0R_1}{(1+\alpha_5)(1+\alpha_6)}\,, \tag{45}$$
$$b_{\varphi 1} = \left(\frac{(2n-\epsilon_2)nR_1}{(3+\alpha_1)\left((2+\alpha_4)-\alpha_3(\frac{3+2\alpha_4}{1+2\alpha_3})^2\right)}\right)^{\frac{1}{2}}\,, \tag{46}$$
$$b_{z1} = -\frac{(3+2\alpha_4)(-\alpha_3)^{\frac{1}{2}}}{(1+2\alpha_3)(1+\alpha_4)^{\frac{1}{2}}}b_{\varphi 1}, \tag{47}$$
$$b_{\varphi 0} = \frac{(3+\alpha_1)R_0}{(2+\alpha_4)R_1}b_{\varphi 1}, \qquad b_{z0} = (-\frac{1+\alpha_4}{\alpha_3})^{\frac{1}{2}}b_{\varphi 0}. \tag{48}$$

Asymptotic solutions (35)–(40) are useful when performing numerical integrations to obtain similarity solutions starting from $\eta \longrightarrow 0$. Now Equations (15)–(20) can be solved by using the asymptotic behaviors.

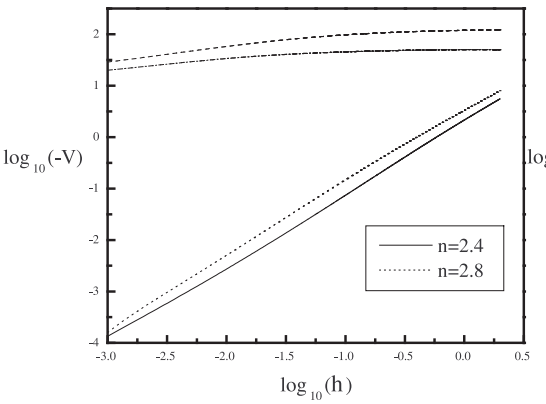

Fig. 8 Velocity distribution in the similarity solution for the case $R_0 = 250$ and $V_1 = 100$, which shows the effect of the cooling function. The dashed and the dot-dashed lines are the curved magnetosonic critical lines.

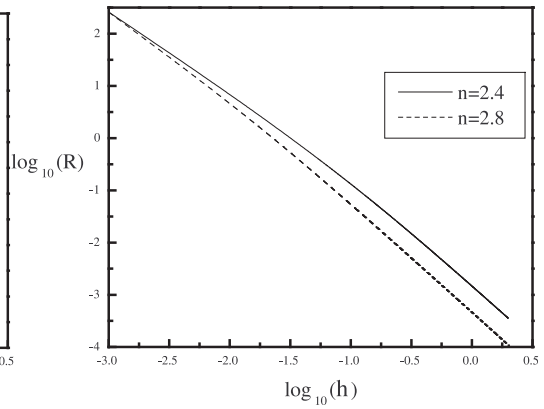

Fig. 9 Density profile corresponding to $R_0 = 250$ and $V_1 = 100$.

Regarding Figure 8, it is observed that even though we proceed from the inner region of the filament to the outer region, as ν increases (i.e. when more energy is released from the filament), infall velocity increases, which is consistent with the result in Section 5.

In Figures 4, 7 and 8, we have shown the radial velocity profiles and magnetosonic lines. The above two lines in these Figures correspond to magnetosonic lines. The curved magnetosonic critical lines and the curved lines of infall velocity do not intersect, so we do not observe any singularity. Consequently, these two methods of integration give consistent results.

Figure 9 shows the value of the density which decreases from the center of the filament to the outer region which is consistent with observations. This decreasing trend also happens with increasing ν.

7 SUMMARY AND DISCUSSION

In this work we consider the evolution of a magnetized self-gravitating filamentary molecular cloud by using a numerical method and we calculate the effects of different parameters on the evolution of the cloud. The magnetic field was assumed to have toroidal and axial components. It is obvious that the magnetic field has a great effect on evolution of the cloud and variations in it can result in a change in the filament structure that acts as a braking effect.

We found that, in the magnetized filamentary cloud, the magnitude of the magnetic field increases in the central region, which is consistent with the latest works and observations (Hennebelle et al. 2008; Chapman et al. 2011). Also, increasing strength of the toroidal component of the magnetic field in the outer region causes an increase in the magnetic field in the central region that should lead to a decrease in the infall velocity which implies magnetic braking occurs. These results are confirmed by Figure 4. In addition, increases in the density of the central region are similar to behavior of the magnetic field, indicating the magnetic field freezes. All of these parameters are related to each other and a change in one can affect the others.

The increase in ν leads to an increase in the cooling function which can be interpreted as more energy release. We expect that increasing the energy released causes an increase in the infall velocity, which is confirmed in Figure 6.

In agreement with Nakajima & Hanawa (1996), we found that the magnetic field in the central region tends to be aligned with the filament axis. This can affect the fragmentation of the cloud which can be studied in future works. The self-similar solution of our model is also in good agreement with the solution in Shadmehri (2005) who found a self-similar solution with only toroidal magnetic fields. It can be observed that considering the magnetic field components, b_z and b_φ, the value of the two components increases in the central regions, which it is consistent with the works of Nakajima & Hanawa (1996), Tilley & Pudritz (2003) and Shadmehri (2005).

We use observational data as the initial conditions of the equations describing the system, then perform a numerical integration from the outer to inner regions and plot the varying behavior of the physical quantities. To consider the accuracy of these results, we again try to integrate the system of ODEs from the inner to the outer regions of the cloud through the use of asymptotic behavior of the derived ODEs in the limit of $\eta \rightarrow 0$. The results derived from these two methods of integration are consistent with each other.

The present model has some limitations. For example, we ignored the rotational velocity of the cloud. However, the rotation should be an important factor for the collapse process (Hennebelle 2003; Krasnopolsky & Königl 2002). Thus the present model that incorperates rotational velocity is an interesting subject for future research.

Acknowledgements We appreciate the anonymous referee for providing very useful comments that helped us to improve the initial version of the paper.

References

Bally, J. 1989, in Proc. ESO Workshop on Low Mass Star Formation and Pre-main-Sequence Objects, 33, ed. B. Reipurth (ESO, Garching), 1
Chandrasekhar, S., & Fermi, E. 1953, ApJ, 118, 116
Chapman, N. L., Goldsmith, P. F., Pineda, J. L., et al. 2011, ApJ, 741, 21
Crutcher, R. M., Roberts, D. A., Troland, T. H., & Goss, W. M. 1999, ApJ, 515, 275
Ferrière, K. 2009, A&A, 505, 1183
Fiege, J. D., & Pudritz, R. E. 2000, MNRAS, 311, 85
Goldsmith, P. F. 2001, ApJ, 557, 736
Hennebelle, P. 2003, A&A, 397, 381
Hennebelle, P., Banerjee, R., Vázquez-Semadeni, E., Klessen, R. S., & Audit, E. 2008, A&A, 486, L43
Henshaw, J. D., Caselli, P., Fontani, F., et al. 2013, MNRAS, 428, 3425
Klessen, R. S., & Burkert, A. 2000, ApJS, 128, 287
Krasnopolsky, R., & Königl, A. 2002, ApJ, 580, 987
Larson, R. B. 1985, MNRAS, 214, 379
Li, D., & Goldsmith, P. F. 2003, ApJ, 585, 823
Li, D., & Goldsmith, P. F. 2012, ApJ, 756, 12
Lou, Y.-Q., & Shen, Y. 2004, MNRAS, 348, 717
Miettinen, O., & Harju, J. 2010, A&A, 520, A102
Miyama, S. M., Narita, S., & Hayashi, C. 1987, Progress of Theoretical Physics, 78, 1051
Moneti, A., Pipher, J. L., Helfer, H. L., McMillan, R. S., & Perry, M. L. 1984, ApJ, 282, 508
Myers, P. C., & Goodman, A. A. 1988a, ApJ, 326, L27
Myers, P. C., & Goodman, A. A. 1988b, ApJ, 329, 392
Nagasawa, M. 1987, Progress of Theoretical Physics, 77, 635
Nakajima, Y., & Hanawa, T. 1996, ApJ, 467, 321
Nakamura, F., Hanawa, T., & Nakano, T. 1995, ApJ, 444, 770
Nakamura, F., Matsumoto, T., Hanawa, T., & Tomisaka, K. 1999, ApJ, 510, 274
Opher, M., Bibi, F. A., Toth, G., et al. 2009, Nature, 462, 1036
Ostriker, E. C., Stone, J. M., & Gammie, C. F. 2001, ApJ, 546, 980
Poidevin, F., Bastien, P., & Jones, T. J. 2011, ApJ, 741, 112
Schneider, N., Csengeri, T., Bontemps, S., et al. 2010, A&A, 520, A49
Shadmehri, M. 2005, MNRAS, 356, 1429
Spitzer, L. 1978, Physical Processes in the Interstellar Medium (New York: Wiley)
Stodólkiewicz, J. S. 1963, Acta Astronomica, 13, 30
Strom, S. E., Strom, K. M., & Edwards, S. 1988, in NATO ASIC Proc. 232, Galactic and Extragalactic Star Formation, eds. R. E. Pudritz, & M. Fich (Dordrecht: Kluwer), 53
Tilley, D. A., & Pudritz, R. E. 2003, ApJ, 593, 426
Uchida, Y. 1989, in Proc. ESO Workshop on Low Mass Star Formation and Pre-main-Sequence Objects, 33, ed. B. Reipurth, 141
Uchida, Y., Fukui, Y., Minoshima, Y., Mizuno, A., & Iwata, T. 1991, Nature, 349, 140
Vrba, F. J., Coyne, G. V., & Tapia, S. 1981, ApJ, 243, 489
Vrba, F. J., Strom, S. E., & Strom, K. M. 1976, AJ, 81, 958
Yu, C., & Lou, Y.-Q. 2005, MNRAS, 364, 1168